Schmidt-number benchmarks for continuous-variable quantum devices

Ryo Namiki

Institute for Quantum Computing and Department of Physics and Astronomy, University of Waterloo, Waterloo, Ontario N2L 3G1, Canada

(Received 25 November 2015; revised manuscript received 26 April 2016; published 26 May 2016)

We present quantum fidelity benchmarks for continuous-variable (CV) quantum devices to outperform quantum channels which can transmit at most k-dimensional coherences for positive integers k. We determine an upper bound of an average fidelity over Gaussian distributed coherent states for quantum channels whose Schmidt class is k. This settles fundamental fidelity steps where the known classical limit and quantum limit correspond to the two end points of $k = 1$ and $k = \infty$, respectively. It turns out that the average fidelity is useful to verify to what extent an experimental CV gate can transmit a high-dimensional coherence. The result is further extended to be applicable to general quantum operations or stochastic quantum channels. Although the fidelity is often associated with heterodyne measurements in quantum optics, we can also obtain similar criteria based on quadrature deviations determined via homodyne measurements.

DOI: 10.1103/PhysRevA.93.052336

I. INTRODUCTION

It is a fundamental question how to generate and characterize higher-dimensional entanglement on quantum systems [1,2]. A central tool to identify higher-dimensional entanglement is the Schmidt number [3]. It is a convex roof extension of the Schmidt rank for pure bipartite quantum states, i.e., the rank of marginal density operators. A quantum state of a Schmidt-class k implies the state can be expressed as a mixture of pure states whose Schmidt rank is at most k for $k = 1,2,3,\ldots$. On the level of quantum channels, the Schmidt-class k implies that there exists a Kraus representation in which the maximum rank of Kraus operators is at most k [4–6]. A channel of Schmidt-class k is also referred to as k-partially entanglement breaking (k-PEB) since it represents an important class of completely positive (CP) maps called entanglement breaking in the case of $k = 1$ [7,8]. The notion of the Schmidt number tells us a precise meaning of the dimensionality in the quantum object and enables us to demonstrate multilevel coherences of quantum gates [9] as well as to verify higher-order entanglement in practical conditions [10–18].

Quantum continuous-variable (CV) systems play a central role in quantum optics and experimental quantum information science [19–21]. They are described by a set of bosonic field operators and capable of simulating any finite-dimensional quantum information process in principle. However, their versatility could be limited due to various imperfections in experiments and is not necessarily accessible in the original form of the theoretical model. Hence, it is natural to ask to what extent a given CV system is capable of simulating a higher-dimensional quantum information process in practice. Notably, a verification scheme of higher-dimensional entanglement of CV quantum states has been proposed [15,17]. However, how to verify higher-dimensional gate coherences in CV quantum gates has not been studied much.

A practical measure to show a basic performance of CV gates [22–24] is an average fidelity over an input ensemble of Gaussian distributed coherent states [25–28]. As an ultimate limitation of gate performance, the quantum limit fidelity was determined in Refs. [29,30]. On the other hand, the entanglement-breaking limit fidelity, which is normally referred to as the classical limit fidelity, was determined in Refs. [26,27,30–33] and established a practical quantum benchmark for CV gates. Similar to other quantum benchmarks [34–39], the fidelity-based benchmark enables us to eliminate the possibility that the process is described by entanglement-breaking maps when the experimental fidelity is higher than the classical limit. Therefore, it can ensure the existence of the coherence in the lowest order of $k = 2$ but could not provide evidence of substantially higher-order coherences expected in CV gates.

Typically, we consider a higher fidelity implies a better gate performance, and it is likely that a higher fidelity suggests a higher Schmidt number and a higher-order coherence. Therefore, an essential question is how high the fidelity need to be in order to outperform a wider class of lower-dimensional processes which belong to the Schmidt class of a given Schmidt-number k. Although the known Schmidt-number benchmarks [9,33] could be usable in general, it is crucial to observe the gate performance using more accessible quantum optical measurements [40]. There are other possibilities to assess the gate coherence quantitatively by using different measures of entanglement [40–43].

In this paper, we present Schmidt-number benchmarks for CV quantum devices based on an average fidelity over Gaussian distributed coherent states. We show an upper bound of the average fidelity achieved by k-PEB channels for any given positive integer k. It gives general fidelity steps that reproduce the classical limit and quantum limit for $k = 1$ and $k = \infty$, respectively. Surpassing the kth limit assesses the existence of $(k + 1)$-dimensional coherences on quantum channels and operations. We also provide a simple conjectural form of the tight kth limit. This conjectured bound is partly achieved by a quantum channel with Schmidt-class k and fully achievable by a probabilistic gate with Schmidt-class k for every k. Furthermore, the fidelity bound is utilized to provide a different form for Schmidt-number benchmarks testable by using homodyne measurements.

The remainder of this paper is organized as follows. In Sec. II, we define the Schmidt-class-k limit of the average fidelity for Gaussian distributed coherent states and show how to find an upper bound. In Sec. III, we extend the resultant fidelity-based benchmarks for probabilistic quantum channels.

In Sec. IV, we show a lower bound of an average quantum noise of canonical quadrature variables to outperform k-PEB operations as well as k-PEB channels. In Sec. V, we conclude this paper with remarks.

II. SCHMIDT-CLASS-k FIDELITY LIMITS FOR QUANTUM CHANNELS

A. Ansatz

We consider transmission of coherent states $|\alpha\rangle := D(\alpha)|0\rangle = e^{-|\alpha|^2/2}\sum_{n=0}^{\infty}\alpha^n|n\rangle/\sqrt{n!}$ through a quantum channel $\mathcal{E}$. Let us consider a transformation task on coherent states $\{|\alpha\rangle\} \to \{|\sqrt{\eta}\alpha\rangle\}$ with $\eta > 0$ and define the average fidelity for Gaussian distributed coherent states as [25–27]

$$F_{\eta,\lambda}(\mathcal{E}) := \int p_\lambda(\alpha)\langle\sqrt{\eta}\alpha|\mathcal{E}(|\alpha\rangle\langle\alpha|)|\sqrt{\eta}\alpha\rangle d^2\alpha, \tag{1}$$

where $p_\lambda(\alpha) = \frac{\lambda}{\pi}\exp(-\lambda|\alpha|^2)$ with $\lambda > 0$. We define the Schmidt-class-k fidelity limit of quantum channels by

$$F^{(k)}(\eta,\lambda) := \max_{\mathcal{E}\in\mathcal{O}_k} F_{\eta,\lambda}(\mathcal{E}), \tag{2}$$

where $\mathcal{O}_k$ is the set of k-PEB channels [4–6]. This set can be defined in terms of Kraus operators $\sum_i K_i^\dagger K_i = \mathbb{1}$ as

$$\mathcal{O}_k = \left\{\mathcal{E}|\mathcal{E}(\rho) = \sum_i K_i\rho K_i^\dagger \wedge \forall\, i,\ \mathrm{rank}(K_i) \leqslant k\right\}. \tag{3}$$

Note that $\mathcal{O}_1$ represents the set of entanglement-breaking channels and $F^{(1)}$ corresponds to the classical limit fidelity [26,27]. Note also that $\mathcal{O}_\infty$ forms the set of whole trace-preserving CP maps and $F^{(\infty)}$ corresponds to the quantum limit fidelity [29]. Therefore, $F^{(k)}$ of Eq. (2) presents unified fidelity steps which include the classical limit and quantum limit as the two end points $k = 1$ and $k = \infty$. Our main goal is to find a nontrivial upper bound of $F^{(k)}$ for every integer $k \in [2,\infty)$.

Note that there is a general definition of PEB channels for CV systems [44]. How to incorporate this general definition into our approach is beyond the scope of this paper.

B. Fidelity bounds

In order to find an upper bound of the fidelity $F^{(k)}$, we introduce a pair of two-mode states [29,31] as

$$\rho_{\mathcal{E}} := \mathcal{E}\otimes I(|\psi_\xi\rangle\langle\psi_\xi|), \tag{4}$$

$$M := \int p_s(\alpha)|\alpha\rangle\langle\alpha|\otimes|\kappa\alpha^*\rangle\langle\kappa\alpha^*|d^2\alpha, \tag{5}$$

where I denotes the identity process, $|\psi_\xi\rangle = \sqrt{1-\xi^2}\sum_{n=0}^{\infty}\xi^n|n\rangle|n\rangle$ is a two-mode squeezed state with $\xi \in (0,1)$, and we assume $s,\kappa > 0$. Using the relation $\langle\alpha|\psi_\xi\rangle = \sqrt{1-\xi^2}e^{-(1-\xi^2)|\alpha|^2/2}|\xi\alpha^*\rangle$ we can find a state-based representation of the fidelity in Eq. (1) as

$$F_{1/N,\tau/N}(\mathcal{E}) = \frac{s+(1-\xi^2)\kappa^2}{s(1-\xi^2)}\mathrm{Tr}\,(\rho_{\mathcal{E}}M), \tag{6}$$

where the parameters (N,τ) in the fidelity function are determined by

$$\tau = s + (1-\xi^2)\kappa^2, \quad N = \kappa^2\xi^2. \tag{7}$$

From Eqs. (2) and (6) we have

$$F^{(k)}(1/N,\tau/N) = \frac{s+(1-\xi^2)\kappa^2}{s(1-\xi^2)}\max_{\mathcal{E}\in\mathcal{O}_k}\mathrm{Tr}\,(\rho_{\mathcal{E}}M). \tag{8}$$

If $\mathcal{E}$ is a k-PEB channel, $\rho_{\mathcal{E}} = \mathcal{E}\otimes I(|\psi_\xi\rangle\langle\psi_\xi|)$ is a state of Schmidt-class k. This implies that the term $\max_{\mathcal{E}\in\mathcal{O}_k}\mathrm{Tr}\,(\rho_{\mathcal{E}}M)$ in Eq. (8) can be upper bounded as

$$\max_{\mathcal{E}\in\mathcal{O}_k}\mathrm{Tr}\,(\rho_{\mathcal{E}}M) \leqslant \max_{\phi\in S_k}\langle\phi|M|\phi\rangle, \tag{9}$$

where S_k denotes the set of pure states whose Schmidt rank is k or less than k.

To proceed, we use the fact that M is invariant under the collective rotation $e^{i\theta(\hat{n}_b-\hat{n}_a)}$. Here, $\hat{n}_a$ ($\hat{n}_b$) stands for the number operator of the first (second) mode. This implies that M can be decomposed into the direct-sum form associated with the eigenspaces of the relative photon-number operator $\hat{n}_b - \hat{n}_a = \sum_J J\mathbb{1}^{(J)}$ as

$$M = \sum_{J=-\infty}^{\infty}\mathbb{1}^{(J)}M\mathbb{1}^{(J)} =: \bigoplus_{J=-\infty}^{\infty}M^{(J)}, \tag{10}$$

where the identities of the orthogonal subspaces can be written as $\mathbb{1}^{(J)} = \sum_{n=0}^{\infty}|e_n^{(J)}\rangle\langle e_n^{(J)}|$ with $|e_n^{(J)}\rangle := |n\rangle|n+J\rangle$ for $J \geqslant 0$ and $|e_n^{(J)}\rangle := |n-J\rangle|n\rangle$ for $J < 0$. As a consequence, an explicit form for $M^{(J)}$ is given by

$$M^{(J)} = \frac{s}{(1+s+\kappa^2)}\sum_{n,m=0}^{\infty}\gamma_{n,m}^{(J)}|e_n^{(J)}\rangle\langle e_m^{(J)}|, \tag{11}$$

where we define

$$\gamma_{n,m}^{(J)} := \frac{(n+m+|J|)!\kappa^J x^{n+m+|J|}}{\sqrt{n!m!(n+|J|)!(m+|J|)!}} \tag{12}$$

and

$$x = \frac{\kappa}{1+s+\kappa^2} \leqslant \frac{1}{2}. \tag{13}$$

From this decomposition and Theorem 2 of Ref. [15], we can see that a Schmidt-number-k vector $|\phi\rangle = \sum a_n|e_n^{(J)}\rangle$ in support of $M^{(J)}$ solves the Schmidt-number-eigenvalue problem of M. This implies that an upper bound is given by comparing the maximum on each subspace,

$$\max_{\psi\in S_k}\langle\phi|M|\phi\rangle = \max_J\max_{\phi\in S_k}\mathrm{Tr}(M^{(J)}|\phi\rangle\langle\phi|). \tag{14}$$

Now, concatenating Eqs. (8), (9), (11), (14) and taking the limit $s \to 0$ with the help of Eq. (7) we obtain

$$F^{(k)}(1/N,\tau/N) \leqslant \frac{N+\tau}{1+N+\tau}\max_J\max_{\phi\in S_k}\langle\phi|A^{(J)}|\phi\rangle, \tag{15}$$

where

$$A^{(J)} := \sum_{n,m=0}^{\infty}\gamma_{n,m}^{(J)}|e_n^{(J)}\rangle\langle e_m^{(J)}|, \tag{16}$$

and $\gamma^{(J)}$ is given by Eq. (12) with $\kappa = \sqrt{N+\tau}$ and $x = \sqrt{N+\tau}/(1+N+\tau)$. Note that, for $\kappa \geqslant 1$ ($\kappa < 1$), the optimization over $J \geqslant 0$ ($J \leqslant 0$) is sufficient due to the relation $\kappa^{-J}\gamma^{(J)}_{n,m} = \kappa^{J}\gamma^{(-J)}_{n,m}$ or equivalently $\kappa^{-J}A^{(J)} = \kappa^{J}A^{(-J)}$.

Since $A^{(J)}$ of Eq. (16) is essentially the same form as L of Eq. (63) in Ref. [15], we can evaluate $\max_{\phi\in S_k}\langle\phi|A^{(J)}|\phi\rangle$ by the maximal eigenvalue of all $(k\times k)$-principal submatrices of $A^{(J)}$. This enables us to determine an upper bound of $F^{(k)}$ as follows. Let us write a $(k\times k)$-principal submatrix of $A^{(J)}$ by

$$A^{(J)}_{\vec{n}} := \sum_{n,m\in\vec{n}} \left|e^{(J)}_n\right\rangle\!\left\langle e^{(J)}_n\right|A^{(J)}\left|e^{(J)}_m\right\rangle\!\left\langle e^{(J)}_m\right|, \tag{17}$$

where $\vec{n} = \{n_1, n_2, \ldots, n_k\}$ is a set of non-negative integers in increasing order, $n_l < n_{l'}$ with $l < l'$, and the number of elements is denoted by $|\vec{n}| = k$. Then, we can formally express the fidelity bound as

$$F^{(k)}(1/N,\tau/N) \leqslant \frac{N+\tau}{1+N+\tau}\max_J \max_{|\vec{n}|=k}\left\|A^{(J)}_{\vec{n}}\right\| =: U_k, \tag{18}$$

where $\|\cdot\|$ denotes the maximum eigenvalue.

The right-hand-side formula of Eq. (18) still involves optimizations over the integer J and the choice of the k-tuple $\vec{n}$. Fortunately, we can find the maximum by checking a finite set of finite-size matrices once the parameters (k,N,τ) are fixed. This is because $\{A^{(J)}\}_J$ is essentially equivalent to the density matrix for the Gaussian state M in the number basis and the contribution involving sufficiently large photon-number elements is negligible. A practical process to determine the maximum is given in the appendices. Eventually, we can find the maximum by filtering out the submatrices whose maximal eigenvalue is smaller than that of another submatrix. In Appendix A, the optimal set $\vec{n}$ is identified for a couple of smaller k's in the case of $J = 0$. Appendix B generalizes the approach presented in Appendix A and gives a systematic process to determine the maximum over general $(J,\vec{n})$ for any given integer $k \in [1,\infty)$.

C. Numerical results and application

Based on the method described in Appendix B, we can numerically determine the upper bound of $F^{(k)}$ in Eq. (18). Figure 1 shows our bound of $F^{(k)}(\eta,\lambda)$ for $k = \{1,2,\ldots,10\}$ and $\eta \in \{0.5,0.75,1.0,1.5,2.0\}$ with $\lambda = 0.01$. For each pair of the parameters $\{\eta,\lambda\}$, surpassing the bound of k implies that the channel $\mathcal{E}$ outperforms k-PEB channels of Eq. (3) and is capable of transmitting entanglement of Schmidt-rank $k+1$. It certifies the quantum coherence unachievable by any teleportation-based quantum gate employing entanglement of Schmidt-class k [6]. The fidelity steps agree with our intuition that a higher fidelity means an existence of stronger entanglement in terms of the Schmidt number and would be widely useful to evaluate the performance of CV quantum gates.

Lobino *et al.* [24] showed an experimental average fidelity as a function of λ for unit-gain $\eta = 1$. In the inset of Fig. 1 we find that the experimental fidelities are located in between the lines $k = 1$ and $k = 2$ and not high enough to demonstrate $k = 3$ or higher-dimensional coherences. This suggests that CV experiments are rather behind demonstrating genuinely higher-dimensional coherences compared with experiments for multiqubit channels [9]. It might be worth noting that the current fidelity record 83% for an experiment of a unit-gain teleportation protocol is a fidelity for an input of the vacuum state [45,46]. This corresponds to the case of $\lambda = \infty$ in our footing and is useless for a verification of the multilevel coherence.

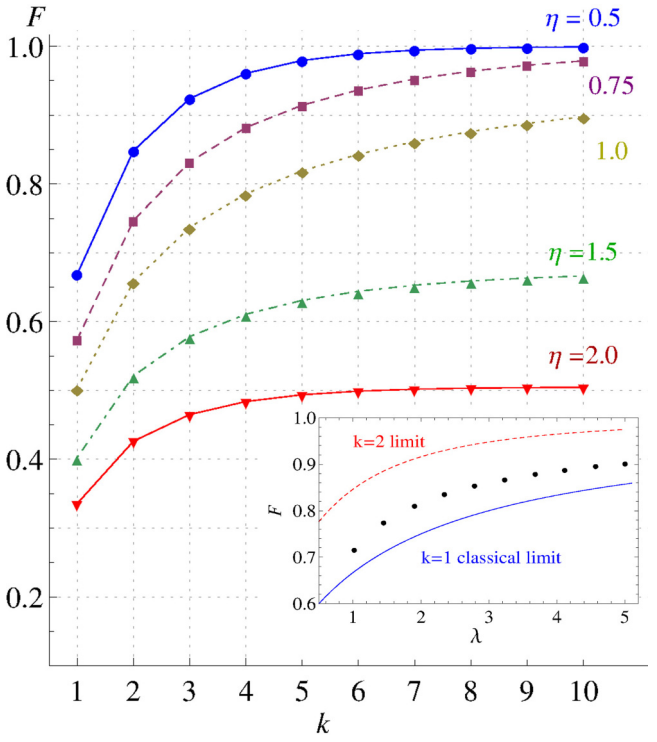

FIG. 1. Our upper bound of the Schmidt-class-k fidelity $F^{(k)}(\eta,\lambda)$ [U_k of Eq. (18)] for $\lambda = 0.01$ and $\eta \in \{0.5,0.75,1.0,1.5,2.0\}$. If an experimental fidelity $F_{\eta,\lambda}(\mathcal{E})$ stays above the kth bound, the experimental CV gate $\mathcal{E}$ cannot be described by a k-PEB channel. This certifies an existence of the $(k+1)$th coherence in the CV gate $\mathcal{E}$. The classical limit fidelity of the fundamental quantum benchmark corresponds to the bound of $k = 1$. In the inset, the classical limit fidelity ($k = 1$) and the fidelity bound for $k = 2$ due to the right-hand side of Eq. (20) are shown as a function of the Gaussian inverse width λ for the case of unit-gain condition $\eta = 1$. The dots represent the average fidelity $F_{1,\lambda}$ given in Fig. 5 of Ref. [24]. This experimental fidelity is not high enough to give evidence to outperform an arbitrary qubit gate with regard to our criterion.

D. Conjecture and attainability

From the numerical results, it has been observed that the largest eigenvalue is given by the first $k\times k$ submatrix $A^{(0)}_{\{0,1,\ldots,k-1\}}$, namely, $\max_J \max_{|\vec{n}|=k}\|A^{(J)}_{\vec{n}}\| = \|A^{(0)}_{\{0,1,\ldots,k-1\}}\|$. Moreover, we can reproduce the expressions of the classical limit [27,31] and the quantum limit [29] from the subspace of $J = 0$ for $k = 1$ and $k = \infty$. To be concrete, it holds that

$$F^{(1)}(1/N,\tau/N) = \frac{N+\tau}{1+N+\tau}\left\|A^{(0)}_{\{0\}}\right\| = \frac{N+\tau}{1+N+\tau},$$

$$F^{(\infty)}(1/N,\tau/N) \leqslant \frac{N+\tau}{1+N+\tau}\left\|A^{(0)}\right\| = \frac{(N+\tau+1)-|N+\tau-1|}{2}. \quad (19)$$

We thus make a conjecture that the general limit is given by a significantly simple form

$$F^{(k)}(1/N,\tau/N) \leqslant \frac{N+\tau}{1+N+\tau}\left\|A^{(0)}_{\{0,1,\ldots,k-1\}}\right\|. \quad (20)$$

Regarding the tightness of this conjectured bound, we present a k-PEB channel which saturates the inequality of Eq. (20) when $\tau \to 0$. Let us define a k-PEB channel $\mathcal{E}^{(k)}(\rho) = \int d^2\alpha\, K^{(k)}_\alpha \rho (K^{(k)}_\alpha)^\dagger$ with Kraus operators of rank k or less than k,

$$K^{(k)}_\alpha := \frac{1}{\sqrt{\pi}} D\left(\frac{\sqrt{\eta}\alpha}{1+\lambda}\right)\left(\sum_{n=0}^{k-1} a^{(k)}_n |n\rangle\langle n|\right) D^\dagger(\alpha). \quad (21)$$

It fulfills $\int d^2\alpha (K^{(k)}_\alpha)^\dagger K^{(k)}_\alpha = \mathbb{1}$ by imposing the condition $\sum_{n=0}^{k-1} a_n^2 = 1$ and gives a simple form of the fidelity,

$$\lim_{\lambda\to 0} F_{\eta,\lambda}(\mathcal{E}^{(k)}) = \sum_{n,m=0}^{k-1} \frac{a_n a_m \sqrt{\eta}^{n+m}}{n!m!}\left(\frac{-\partial}{\partial\eta}\right)^{n+m}\frac{1}{1+\eta} = \frac{1}{1+\eta}\sum_{n,m=0}^{k-1} a_n \gamma^{(0)}_{n,m} a_m =: f^{(k)}, \quad (22)$$

where $\gamma^{(0)}_{n,m}$ is given by Eq. (12) with $x = \sqrt{\eta}/(1+\eta)$. This implies $\max_{\{a_n\}} f^{(k)} = (1-\eta)^{-1}\|A^{(0)}_{\{0,1,\ldots,k-1\}}\|$ and $\mathcal{E}^{(k)}$ achieves the conjectured bound of Eq. (20) for $\tau = 0$. It was shown that $\mathcal{E}^{(1)}$ achieves the classical limit in Ref. [27]. For $k = 2$ and $k = 3$, we have observed numerically that $\mathcal{E}^{(k)}$ could not achieve the limit when $\tau > 0$. Interestingly, we can generally show that the conjectured fidelity bound in Eq. (20) is achievable by a probabilistic quantum gate of Schmidt-class k for every k (see Sec. III B).

III. EXTENSION FOR GENERAL QUANTUM OPERATIONS

Our benchmarks can be extended for general quantum operations, namely, the trace-non-increasing class of CP maps (see Ref. [33] for a general framework). In Sec. III A we show that the bound U_k of Eq. (18) holds for CP maps of Schmidt-class k with a modified form of the fidelity. Notably, the bound U_k is tight when general quantum operations are taken into account. An interesting example of trace-decreasing CP maps for CV states is the so-called noiseless linear amplifier or probabilistic amplifiers [30,40,47–50]. In Sec. III B, we prove that such a stochastic quantum channel achieves the conjectured bound of Eq. (20).

A. Fidelity bounds for CP maps

Suppose that $\mathcal{E}$ is a quantum operation, namely, a trace-non-increasing CP map. We may modify the definition of the fidelity in Eq. (1) as [30]

$$F_{\eta,\lambda}(\mathcal{E}) := P_s^{-1}\int p_\lambda(\alpha)\langle\sqrt{\eta}\alpha|\mathcal{E}(|\alpha\rangle\langle\alpha|)|\sqrt{\eta}\alpha\rangle d^2\alpha, \quad (23)$$

where $p_\lambda(\alpha) = \frac{\lambda}{\pi}\exp(-\lambda|\alpha|^2)$ with $\lambda > 0$ and $P_s := \mathrm{Tr}\int p_\lambda(\alpha)\mathcal{E}(|\alpha\rangle\langle\alpha|)d^2\alpha$ is the probability that $\mathcal{E}$ gives an output state for the ensemble $\{p_\lambda(\alpha), |\alpha\rangle\langle\alpha|\}$. Note that Eq. (23) reduces to Eq. (1) for the trace-preserving case, i.e., for quantum channels. In fact, $\mathrm{Tr}[\mathcal{E}(|\alpha\rangle\langle\alpha|)] = 1$ for all $\alpha \in \mathbb{C}$ implies $P_s = 1$.

Similar to Eq. (2), let us define the Schmidt-class-k fidelity limit with the renormalized fidelity in Eq. (23) as

$$F^{(k)}(\eta,\lambda) := \max_{\mathcal{E}\in\mathcal{O}_k} F_{\eta,\lambda}(\mathcal{E}), \quad (24)$$

where $\mathcal{O}_k$ denotes the set of k-PEB maps described by $\mathcal{E}(\rho) = \sum_i K_i \rho K_i^\dagger$. Here, operators $\{K_i\}$ have rank k or less than k (we do not impose trace-preserving condition $\sum_i K_i^\dagger K_i = \mathbb{1}$).

In order to show that the same fidelity bound U_k in Eq. (18) holds for quantum operations [33], the key is to employ the normalized state,

$$\rho_\mathcal{E} := \frac{\mathcal{E}\otimes I(|\psi_\xi\rangle\langle\psi_\xi|)}{\mathrm{Tr}[\mathcal{E}\otimes I(|\psi_\xi\rangle\langle\psi_\xi|)]}. \quad (25)$$

By using this formula instead of Eq. (4), the procedure in Sec. II B leads to the fidelity bound for general CP maps,

$$F^{(k)}(\eta,\lambda) \leqslant U_k(\eta,\lambda) = \frac{1+\lambda}{1+\eta+\lambda}\max_J \max_{|\vec{n}|=k}\left\|A^{(J)}_{\vec{n}}\right\|, \quad (26)$$

where $\|\cdot\|$ denotes the maximum eigenvalue and $A^{(J)}_{\vec{n}}$ is defined through Eqs. (12), (16), and (17) with

$$x = \frac{\sqrt{\eta(1+\lambda)}}{1+\eta+\lambda}, \quad \kappa = \sqrt{\frac{1+\lambda}{\eta}}. \quad (27)$$

Note that Eq. (26) is tight, namely, it holds that

$$F^{(k)}(\eta,\lambda) = U_k(\eta,\lambda). \quad (28)$$

This can be confirmed from the fact that U_k is a solution of the Schmidt-number-eigenvalue problem [15] together with the property of k-PEB maps that $\rho_\mathcal{E}$ of Eq. (25) can be any pure state of Schmidt-number k.

For quantum channels (trace-preserving CP maps), it remains open how to find a tight limit except for the classical limit $k = 1$ [27] and quantum limit $k = \infty$ [29,30].

By comparing an experimentally observed fidelity and our upper bound of the kth fidelity limit $F^{(k)}$, one can verify a genuine multidimensional coherence for general quantum operations as well as for quantum channels. To be concrete, we can eliminate the possibility that the physical process $\mathcal{E}$ is described as a k-PEB map if it holds that $F_{\eta,\lambda}(\mathcal{E}) > U_k(\eta,\lambda)$. This establishes an infinite sequence of quantitative quantum benchmarks for general single-mode physical processes with respect to the Schmidt-number k. The fidelity steps $U_k(\eta,\lambda)$ would give distinctive milestones to assess the closeness between an experimental amplifier and an ideal quantum limited amplification process [30,40] by simultaneously observing the Schmidt number and the fidelity.

B. Proof of attainability of the conjectured bound

In Sec. II D, we have conjectured that the simple form in Eq. (20) gives a tighter bound. Here, we will show that a

probabilistic quantum channel of Schmidt-class k achieves the conjectured bound,

$$F^{(k)}(\eta,\lambda) \leqslant \frac{1+\lambda}{1+\eta+\lambda}\left\| A^{(0)}_{\{0,1,\ldots,k-1\}}\right\|. \tag{29}$$

Proof. Let us consider the following filtering operator:

$$Q_k = \sqrt{\mathcal{N}}\sum_{n=0}^{k-1} a_n g^n |n\rangle\langle n|, \tag{30}$$

where $(\mathcal{N},g)$ is a pair of positive constants and we assume $\sum_{n=0}^{k-1}|a_n|^{\,2}=1$. We can readily calculate its action onto coherent states as

$$Q_k|\alpha\rangle = \sqrt{\mathcal{N}}e^{-|\alpha|^2/2}\sum_{n=0}^{k-1}\frac{a_n(g\alpha)^n}{\sqrt{n!}}|n\rangle. \tag{31}$$

Evidently, Q_k is rank k or less than k. This implies that the probabilistic quantum-gate $\mathcal{E}(\rho)=Q_k\rho Q_k^\dagger$ belongs to Schmidt-class k. From these expressions we have

$$\begin{aligned}&\int p_\lambda(\alpha)\langle\sqrt{\eta}\alpha|\mathcal{E}(|\alpha\rangle\langle\alpha|)|\sqrt{\eta}\alpha\rangle d^2\alpha\\ &= \mathcal{N}\lambda\sum_{n,m=0}^{k-1}\frac{(n+m)!}{n!m!}\frac{(\sqrt{\eta}g)^{m+m}a_n a_m^*}{(1+\eta+\lambda)^{n+m+1}}\\ &= \frac{\mathcal{N}\lambda}{1+\eta+\lambda}\sum_{n,m=0}^{k-1}\gamma^{(0)}_{n,m}a_n a_m^*,\end{aligned} \tag{32}$$

where we use $\int p_\lambda(\alpha)e^{-(1+\eta)|\alpha|^2}|\alpha|^{2k}d^2\alpha = \lambda k!/(1+\eta+\lambda)^{k+1}$ for calculating the integration. Moreover, the final expression is obtained by substituting $g=\sqrt{1+\lambda}$ and using the definition of $\gamma^{(0)}_{n,m}$ in Eq. (12) where the parameter x is given by Eq. (27). Note that from the definition of the submatrix $A^{(J)}_{\vec{n}}$ given through Eqs. (12), (16), and (17), we can write

$$\max\left(\sum_{n,m=0}^{k-1}\gamma^{(0)}_{n,m}a_n a_m^*\right) = \left\|A^{(0)}_{\{0,1,\ldots,k-1\}}\right\|, \tag{33}$$

where the maximum is taken over $\sum_{n=0}^{k-1}|a_n|^2=1$.

On the other hand, the relation in Eq. (31) and the condition $g=\sqrt{1+\lambda}$ yield the following expression:

$$\begin{aligned}P_s &= \mathrm{Tr}\int p_\lambda(\alpha)\mathcal{E}(|\alpha\rangle\langle\alpha|)d^2\alpha\\ &= \mathcal{N}\lambda\sum_{n=0}^{k-1}\frac{|a_n|^2 g^{2n}}{(1+\lambda)^{n+1}}\\ &= \frac{\mathcal{N}\lambda}{1+\lambda}\sum_{n=0}^{k-1}|a_n|^2 = \frac{\mathcal{N}\lambda}{1+\lambda}.\end{aligned} \tag{34}$$

From Eqs. (23), (32), and (34) we obtain

$$F_{\eta,\lambda}(\mathcal{E}) = \frac{1+\lambda}{1+\eta+\lambda}\sum_{n,m=0}^{k-1}\gamma^{(0)}_{n,m}a_n a_m^*. \tag{35}$$

Finally, optimizing the coefficient $\{a_n\}$ of the filter Q_k as in Eq. (33) we can conclude that the right-hand side of Eq. (29) [Eq. (20)] is achievable by a probabilistic quantum gate of Schmidt-class k. ■

Note that the normalization factor $\mathcal{N}$ of Q_k in Eq. (30) can be positive as long as k is finite. This fact confirms the attainability with a finite success probability $P_s>0$. In the limit of $k\to\infty$, however, $\mathcal{N}$ could be zero so as to fulfill the physical condition $Q_k^\dagger Q_k \leqslant \mathbb{1}$ (see Refs. [30,40]).

IV. SCHMIDT-CLASS-k LIMITATION ON QUANTUM NOISE OF CANONICAL VARIABLES

In this section, we present a Schmidt-class-k limit on an average of Bayesian mean-square deviations for canonical variables. We introduce a basic relation between the fidelity and the quantum noise in Sec. IV A. Resultant Schmidt-number benchmarks are given in Sec. IV B.

A. Canonical quantum noise and fidelity

Let $\hat{x}$ and $\hat{p}$ be canonical quadrature variables with the canonical commutation relation $[\hat{x},\hat{p}]=i$. The field operator $\hat{a}$ is given as $\hat{a}=(\hat{x}+i\hat{p})/\sqrt{2}$ and satisfies the bosonic commutation relation $[\hat{a},\hat{a}^\dagger]=1$. For notation convention we write the mean quadratures for coherent states as

$$x_\alpha := \langle\alpha|\hat{x}|\alpha\rangle = \frac{\alpha+\alpha^*}{\sqrt{2}}, \quad p_\alpha := \langle\alpha|\hat{p}|\alpha\rangle = \frac{\alpha-\alpha^*}{\sqrt{2}i}. \tag{36}$$

Let $\mathcal{E}$ be a quantum operation. We define the mean-square deviations for canonical quadratures [27,39,40] as

$$\bar{V}_z := P_s^{-1}\mathrm{Tr}\left[\int p_\lambda(\alpha)(\hat{z}-\sqrt{\eta}z_\alpha)^2\mathcal{E}(|\alpha\rangle\langle\alpha|)d^2\alpha\right], \tag{37}$$

where $z\in\{x,p\}$, $p_\lambda(\alpha):=\frac{\lambda}{\pi}\exp(-\lambda|\alpha|^2)$, and $P_s := \mathrm{Tr}\int p_\lambda(\alpha)\mathcal{E}(|\alpha\rangle\langle\alpha|)d^2\alpha$. With the help of the property of the displacement operator $D(\alpha)\hat{a}D^\dagger(\alpha)=\hat{a}-\alpha$ and the cyclic property of the trace, we can write

$$\begin{aligned}\bar{V}_z &= P_s^{-1}\mathrm{Tr}\left[\int p_\lambda(\alpha)D(\sqrt{\eta}\alpha)\hat{z}^2D^\dagger(\sqrt{\eta}\alpha)\mathcal{E}(|\alpha\rangle\langle\alpha|)d^2\alpha\right]\\ &= P_s^{-1}\mathrm{Tr}[\hat{z}^2\sigma],\end{aligned} \tag{38}$$

where we defined

$$\sigma := \int p_\lambda(\alpha)D^\dagger(\sqrt{\eta}\alpha)\mathcal{E}(|\alpha\rangle\langle\alpha|)D(\sqrt{\eta}\alpha)d^2\alpha. \tag{39}$$

Note that we can readily confirm the following relations:

$$\begin{aligned}\mathrm{Tr}[\sigma] &= \mathrm{Tr}\int p_\lambda(\alpha)\mathcal{E}(|\alpha\rangle\langle\alpha|)d^2\alpha\\ &= P_s,\\ \langle 0|\sigma|0\rangle &= \int p_\lambda(\alpha)\langle\sqrt{\eta}\alpha|\mathcal{E}(|\alpha\rangle\langle\alpha|)|\sqrt{\eta}\alpha\rangle d^2\alpha.\end{aligned} \tag{40}$$

From Eq. (38) and the well-known expression for the harmonic oscillator $\hat{x}^2+\hat{p}^2=2\hat{a}^\dagger\hat{a}+1$, the sum of the mean-square deviations can be expressed as

$$\bar{V}_x+\bar{V}_p = \frac{1}{P_s}(2\,\mathrm{Tr}[\hat{a}^\dagger\hat{a}\sigma]+\mathrm{Tr}[\sigma]). \tag{41}$$

On the other hand, we can show the following inequality for any positive semidefinite operator ρ:

$$\begin{aligned}\mathrm{Tr}[\hat{a}^\dagger\hat{a}\rho] &= \mathrm{Tr}\left(\sum_{n=1}^{\infty} n|n\rangle\langle n|\rho\right)\\ &\geqslant \mathrm{Tr}\left(\sum_{n=1}^{\infty} |n\rangle\langle n|\rho\right)\\ &= \mathrm{Tr}[\rho] - \langle 0|\rho|0\rangle. \end{aligned} \tag{42}$$

Concatenating Eqs. (41)–(42) with $\rho = \sigma$, we obtain the relation between the sum quantum noise and the average fidelity [27],

$$\bar{V}_x + \bar{V}_p - 1 \geqslant \frac{2}{P_s}(\mathrm{Tr}[\sigma] - \langle 0|\sigma|0\rangle) = 2(1 - F_{\eta,\lambda}), \tag{43}$$

where $F_{\eta,\lambda}$ is defined in Eq. (23). From Eq. (43), we can see that a smaller value of quantum noise ensures a higher fidelity. To be concrete, Eq. (43) implies that the fidelity is bounded from below by using the mean-square deviations,

$$F_{\eta,\lambda} \geqslant \frac{3}{2} - \frac{\bar{V}_x + \bar{V}_p}{2}. \tag{44}$$

In particular, we can observe that $F = 1$ if $V_x + V_p = 1$.

B. Schmidt-number benchmarks via quantum noise

Now, we can find a lower bound of the Schmidt number by using the sum of the mean-square deviations V_x and V_p. We can show that $F_{\eta,\lambda}(\mathcal{E}) > F^{(k)}(\eta,\lambda)$ holds if the following condition is satisfied:

$$\bar{V}_x + \bar{V}_p - 1 < 2[1 - F^{(k)}(\eta,\lambda)]. \tag{45}$$

Proof. Suppose Eq. (45) holds. From Eqs. (43) and (45), we have

$$2(1 - F_{\eta,\lambda}) \leqslant \bar{V}_x + \bar{V}_p - 1 < 2[1 - F^{(k)}(\eta,\lambda)]. \tag{46}$$

Comparing the left-end and right-end expressions, we obtain $F_{\eta,\lambda}(\mathcal{E}) > F^{(k)}(\eta,\lambda)$. Hence, Eq. (45) is a sufficient condition that $\mathcal{E}$ outperforms any k-PEB maps. ■

For a practical use, one can replace the term $F^{(k)}$ in Eq. (45) with the upper bound U_k given in Eq. (18). We thus have the following quantum benchmark:

$$\bar{V}_x + \bar{V}_p - 1 < 2[1 - U_k(\eta,\lambda)]. \tag{47}$$

This condition can be readily tested by plugging-in an experimentally observed value of $\bar{V}_x + \bar{V}_p$. Hence, one can verify that the Schmidt number of the process $\mathcal{E}$ is at least $k + 1$ if the inequality of Eq. (47) is fulfilled.

Note that the condition of Eq. (45) is not tight when $k = 1$ (see, Corollary 1 of Ref. [39]) and unlikely to be tight for other choices of $k \geqslant 2$. How to find a better link between the Schmidt class and the quadrature deviations for an improvement of our approach should be addressed elsewhere.

V. CONCLUSION AND REMARKS

In conclusion, we have presented Schmidt-number benchmarks for CV quantum devices using the average fidelity for Gaussian distributed coherent states. Our benchmarks give everlasting fidelity steps towards higher-dimensional quantum-gate coherence and successfully generalize the known classical and quantum limits by recasting them into the two end points of these steps. Our result refines the meaning of "high fidelity" for CV quantum gates, and the numerically determined fidelity steps would be useful to demonstrate genuinely higher-dimensional coherence for experimental implementations. It is fundamentally important to show stronger evidence that CV systems have a potential superiority in dealing with higher-dimensional quantum signals. In this respect, distinctive experimental progress could be regularly quantified and recorded based on the Schmidt class determined by the fidelity steps. We have also conjectured a simple formula for the fidelity bound. This bound is achievable by a probabilistic quantum gate of the corresponding Schmidt class. Furthermore, we have presented a lower bound of an average quantum noise to outperform k-PEB processes. This bound is directly related to homodyne measurements and could provide wider options for an experimental verification of higher-dimensional coherences.

Although our results are readily available as a type of entanglement verification tool for experiments, there are several open possibilities to improve the fidelity bound and the bound for the canonical quantum noise. We recall the following three aspects for an outlook.

(i) Our fidelity bound U_k is tight for quantum operations, yet we have not identified what operation can achieve this bound. (In Sec. III B we have provided a concrete form of a probabilistic gate that achieves the conjectured bound. If the conjectured bound is proven equivalent to U_k, we can immediately settle this problem.)

(ii) How to improve the fidelity bound U_k for the case of quantum channels and how to identify the optimal k-PEB channel which maximizes the fidelity for $k \in [2,\infty)$ remains open. In this regard, it has been known [30] that there is a gap between the quantum limit fidelities ($k \to \infty$) for probabilistic gates and deterministic gates, whereas there is no gap for the classical fidelity limits ($k = 1$). An existence of the gap is crucial to demonstrate an advantage of probabilistic gates [40].

(iii) Aside from the fidelity-based approach, exploring a feasible method based on the statistical moments of canonical variables would be important. As well as improving our bound for the sum of the mean-square deviations in Sec. IV B, an interesting problem is to determine the trade-off relation between the mean-square deviations under the constraint of the Schmidt class. Hopefully, we could prove a general sequence of uncertainty relations for V_x and V_p, which reproduces the uncertainty relation over entanglement-breaking maps for $k = 1$ [39] and approaches the amplification uncertainty relation [40] in the limit $k \to \infty$.

ACKNOWLEDGMENTS

R.N. was supported by the DARPA Quiness program under prime Contract No. W31P4Q-12-1-0017, NSERC, and Industry Canada. This work was partly supported by GCOE Program "The Next Generation of Physics, Spun from Universality and Emergence" from MEXT of Japan.

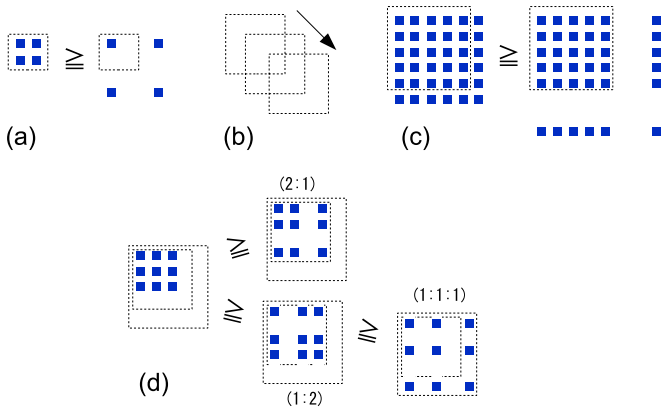

FIG. 2. Orders of principal submatrices.

APPENDIX A: RIGOROUS RESULT FOR THE MAXIMIZATION IN EQ. (18) FOR $J = 0$

As a first step to estimate the maximization in Eq. (18), we consider the case of $J = 0$. In the case of $J = 0$ we can show that the exact maximum for $k \in \{1,2,3\}$ is given by

$$\max_{|\vec{n}|=k} \left\| A^{(0)}_{\vec{n}} \right\| = \left\| A^{(0)}_{\{0,1,\ldots,k-1\}} \right\|. \tag{A1}$$

In order to verify this relation, we use the following two properties for γ defined through Eqs. (12) and (13):

(i) $\gamma^{(0)}_{n+1,n-l+1} - \gamma^{(0)}_{n,n-l} \leqslant 0$ holds for $n \geqslant \frac{1}{2}(l+2)(l-l)$.

(ii) $\gamma^{(0)}_{n+1,m} - \gamma^{(0)}_{n,m} \leqslant 0$ holds for $m \leqslant n-1$.

First, property (i) with $l = 0$ implies that the diagonal elements are in decreasing order, namely, $\gamma^{(0)}_{0,0} \geqslant \gamma^{(0)}_{1,1} \geqslant \gamma^{(0)}_{2,2} \geqslant \cdots$. This proves Eq. (A1) for $k = 1$. Note that property (i) with $l = 1$ implies that the first off-diagonal elements are in decreasing order, namely, it holds that $\gamma^{(0)}_{0,1} \geqslant \gamma^{(0)}_{1,2} \geqslant \gamma^{(0)}_{2,3} \geqslant \cdots$. Similarly, property (i) with $l = 2$ implies that the second off-diagonal elements are in decreasing order, namely, it holds that $\gamma^{(0)}_{0,2} \geqslant \gamma^{(0)}_{1,3} \geqslant \gamma^{(0)}_{2,4} \geqslant \cdots$.

Next, to prove Eq. (A1) for $k = 2$ we show

$$\begin{pmatrix} \gamma^{(0)}_{n,n} & \gamma^{(0)}_{n,n+1} \\ \gamma^{(0)}_{n+1,n} & \gamma^{(0)}_{n+1,n+1} \end{pmatrix} - \begin{pmatrix} \gamma^{(0)}_{n+1,n+1} & \gamma^{(0)}_{n+1,n+2} \\ \gamma^{(0)}_{n+2,n+1} & \gamma^{(0)}_{n+2,n+2} \end{pmatrix} \geqslant 0,$$
$$\begin{pmatrix} \gamma^{(0)}_{n,n} & \gamma^{(0)}_{n,n+1} \\ \gamma^{(0)}_{n+1,n} & \gamma^{(0)}_{n+1,n+1} \end{pmatrix} - \begin{pmatrix} \gamma^{(0)}_{n,n} & \gamma^{(0)}_{n,n+n'} \\ \gamma^{(0)}_{n+n',n+n'} & \gamma^{(0)}_{n+n',n+n'} \end{pmatrix} \geqslant 0, \tag{A2}$$

where each inequality for the matrices indicates all elements are non-negative. The first inequality suggests the decreasing order on shift in the diagonal direction associated with the schematics of Fig. 2(b); the second inequality suggests the decreasing order on spread in the vertical-and-horizontal direction associated with the schematics of Fig. 2(a). The first inequality in Eqs. (A2) is proven from the decreasing order on the diagonal elements and the first off-diagonal elements. The second inequality in Eqs. (A2) is proven by using the decreasing order on the diagonal elements and property (ii). From the inequalities in Eqs. (A2) we have $\|A^{(0)}_{\{n,n+1\}}\| \geqslant \|A^{(0)}_{\{n+1,n+2\}}\|$ and $\|A^{(0)}_{\{n,n+1\}}\| \geqslant \|A^{(0)}_{\{n,n+n'\}}\|$ since $\|a\| \leqslant \|b\|$ holds for non-negative matrices a and b with $0 \leqslant a \leqslant b$ (see Corollary 8.1.19. of Ref. [51]). Using these two relations recursively we can conclude Eq. (A1) for $k = 2$. Note that, from the order of the diagonal elements and property (ii), we can generally obtain such a matrix inequality when the position of the final row and column is shifted as in Fig. 2(c).

Finally, similar to this proof, we proceed to the proof of $k = 3$ by comparing the corresponding submatrix elements associated with $\|A^{(0)}_{\{n,n+1,n+2\}}\| \geqslant \|A^{(0)}_{\{n+1,n+2,n+3\}}\|$ for the diagonal direction shift and $\|A^{(0)}_{\{n,n+1,n+2\}}\| \geqslant \|A^{(0)}_{\{n,n+n',n+n''\}}\|$ for the spreading shift. For the diagonal shift of the 3×3 matrix, the matrix inequality can be confirmed by the decreasing order on the diagonal elements, the first off-diagonal elements, and the second off-diagonal elements, coming from property (i) with $l \in \{0,1,2\}$. For the spreading of the 3×3 matrix, we have three possibilities to divide the elements (2:1), (2:1), and (1:1:1) as in Fig. 2(d). For the case of (2:1), the inequality can be proven by property (ii) and the decreasing order on the diagonal elements. For the case of (1:2), the inequality can be proven by property (ii) and the decreasing order on the diagonal shift of the 2×2 matrix. Then, the first inequality of Eq. (A2) on the 2×2 matrix and the decreasing order on the diagonal elements again enable us to show the decreasing order on the spreading shift from (1:2) to (1:1:1). Therefore, we can conclude that the relation Eq. (A1) holds for $k \in \{1,2.3\}$.

For $k = 4$, we can show the inequality for the spreading shift $\|A^{(0)}_{\{n,n+1,n+2,n+3\}}\| \geqslant \|A^{(0)}_{\{n,n+n',n+n'',n+n'''\}}\|$ by using property (ii) and the results of the 2×2 and 3×3 matrices above. Similarly, from property (i) and the results of $k \leqslant 3$ above we have $\|A^{(0)}_{\{n,n+1,n+2,n+3\}}\| \geqslant \|A^{(0)}_{\{n+1,n+2,n+3,n+4\}}\|$ when $n \geqslant 2$. However, the matrix inequality for the diagonal shift cannot hold for the first two submatrices $A^{(0)}_{\{0,1,2,3\}}$ and $A^{(0)}_{\{1,2,3,4\}}$. Therefore, the maximum is obtained by comparing the first three cases of the matrices, i.e., $\max_{n\in\{0,1,2\}} \|A^{(0)}_{\{n,n+1,n+2,n+3\}}\|$. In this manner, we can eventually determine the maximum by comparing the maximum eigenvalues of a relatively small number of submatrices for a couple of small k's. We present a general systematic approach to determine the maximum of Eq. (18) in the following section.

APPENDIX B: GENERAL RECIPE TO DETERMINE THE MAXIMUM IN EQ. (18)

In the previous section, we use the following two properties to make (matrix) inequalities on submatrices of $A^{(0)}$ defined through Eqs. (12) and (13):

(i) $\gamma^{(0)}_{n+1,n-l+1} - \gamma^{(0)}_{n,n-l} \leqslant 0$ holds for $n \geqslant \frac{1}{2}(l+2)(l-l)$.

(ii) $\gamma^{(0)}_{n+1,m} - \gamma^{(0)}_{n,m} \leqslant 0$ holds for $m \leqslant n-1$.

In this section, we develop this method and present a systematic approach to determine the maximum in Eq. (18). An essential fact to generate matrix inequalities is that $\|a\| \leqslant \|b\|$ holds for non-negative matrices a and b with $0 \leqslant a \leqslant b$ (see Corollary 8.1.19. of Ref. [51]).

Let us note general properties of $A^{(J)}$. (a) $A^{(J)}$ is a non-negative matrix and symmetric, i.e., for any n,m, $\gamma^{(J)}_{n,m} \geqslant 0$, and $\gamma^{(J)}_{n,m} = \gamma^{(J)}_{m,n}$. (b) If $n \geqslant \frac{1}{2}(|J|-2)(|J|+1)$, we have $\gamma^{(J)}_{n+1,n+1} - \gamma^{(J)}_{n,n} \leqslant 0$. (c) The sequence of the diagonal elements

$\{\gamma^{(J)}_{n,n}\}_n$ is at most single peaked, and the largest element is located around $n \sim \frac{1}{2}(|J|^2 - |J| - 2)$. From these properties and the fact that eigenvalues of a positive semidefinite matrix are upper bounded by its trace, we can neglect the contribution from sufficiently large n when we determine the maximum in Eq. (18), numerically.

1. Derivation of properties (i) and (ii)

From Eqs. (12) and (13) we have

$$\gamma^{(J)}_{n+1,m+1} - \gamma^{(J)}_{n,m} \leqslant \gamma^{(J)}_{n,m} \times \left(\frac{(n+m+|J|+2)(n+m+|J|+1)}{\sqrt{(n+1)(m+1)(n+|J|+1)(m+|J|+1)}} \frac{1}{4} - 1 \right). \tag{B1}$$

Suppose that $m = n - l \leqslant n$. If we set $J = 0$, we obtain property (i). In our approach, a key observation is that any lth off-diagonal element gradually gives a decreasing sequence. We define an integer t_l to utilize this fact. The integer t_l that fulfills $\gamma^{(J)}_{n+1,m+1} - \gamma^{(J)}_{n,m} \leqslant 0$ is summarized in Table I for $l \leqslant 10$. The row of $l = 0$ shows all diagonal elements are in decreasing order for $|J| \leqslant 2$. The row of $l = 1$ shows all first off-diagonal elements are in decreasing order for $|J| \leqslant 1$. Note that the values in Table I are determined by taking the worst case of $x = \frac{1}{2}$ (better bounds would be obtained when a specific value of $x < \frac{1}{2}$ is given).

Suppose that $m \leqslant n - 1$. From Eqs. (12) and (13) we have

$$\begin{aligned} \gamma^{(J)}_{n+1,m} - \gamma^{(J)}_{n,m} &\leqslant \gamma^{(J)}_{n,m} \left(\frac{n+m+|J|+1}{\sqrt{(n+1)(n+|J|+1)}} \frac{1}{2} - 1 \right) \\ &\leqslant \gamma^{(J)}_{n,m} \left(\frac{n+|J|/2}{\sqrt{(n+1)(n+|J|+1)}} - 1 \right). \end{aligned} \tag{B2}$$

This implies $\gamma^{(J)}_{n+1,m} - \gamma^{(J)}_{n,m} \leqslant 0$ for $|J| \leqslant 4$. For $|J| > 4$, $\gamma^{(J)}_{n+1,m} - \gamma^{(J)}_{n,m} \leqslant 0$ is fulfilled when

$$n \geqslant (-4 - 4|J| + J^2)/8 =: u^{(J)}. \tag{B3}$$

As a consequence, the case of $J = 0$ gives property (ii). Notably, the expressions derived here suggest that we can use modified versions of properties (i) and (ii) for $J \neq 0$. Our main residual task is to make matrix inequalities systematically based on the general properties of $\{\gamma^{(J)}_{n,m}\}$.

TABLE I. The integer $t^{(J)}_l$ in which lth off-diagonal elements become decreasing order for $|J| \leqslant 4$. The superscript index "(J)" of $t^{(J)}_l$ is omitted through the text.

l	$J=0$	$\lvert J\rvert=1$	$\lvert J\rvert=2$	$\lvert J\rvert=3$	$\lvert J\rvert=4$
0	0	0	0	2	5
1	1	1	2	4	7
2	2	3	4	6	9
3	5	6	7	9	12
4	9	10	11	13	16
5	14	15	16	18	21
6	20	21	22	24	27
7	27	28	29	31	34
8	35	36	37	39	42
9	44	45	46	48	51
10	54	55	56	58	61

2. Inequalities for the diagonal shift

From Table I, we can determine the index n of the diagonal elements of $A^{(J)}$ so that the $(k \times k)$-principal submatrices starting from $[A^{(J)}]_{n,n}$ become decreasing order associated with the diagonal shift of Fig. 3(a). From the rows of $l = 0$ in Table I, we can confirm that the diagonal elements are in decreasing order for $|J| \leqslant 2$. The diagonal elements of $A^{(3)}$ and $A^{(4)}$ are in decreasing order whenever $n \geqslant 2$ and $n \geqslant 5$, respectively. From the rows of $l = 0$ and $l = 1$ in Table I, we can confirm that the relation on the 2×2 submatrices,

$$\begin{pmatrix} \gamma_{n,n} & \gamma_{n,n+1} \\ \gamma_{n+1,n} & \gamma_{n+1,n+1} \end{pmatrix} - \begin{pmatrix} \gamma_{n+1,n+1} & \gamma_{n+1,n+2} \\ \gamma_{n+2,n+1} & \gamma_{n+2,n+2} \end{pmatrix} \geqslant 0$$

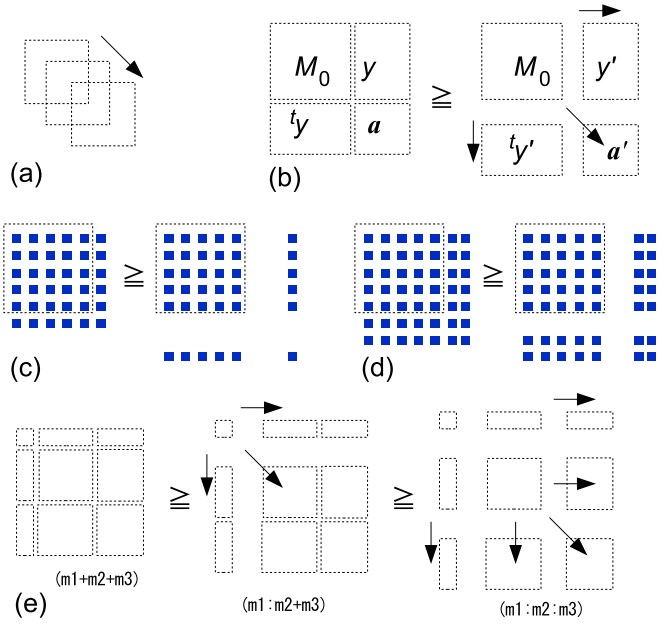

FIG. 3. To determine the order of the maximum eigenvalues of the different submatrices (a) a primitive step is to compare submatrices which can be chosen by shifts on the diagonal direction. (b) Another primitive step is to compare submatrices which have the same elements but some of the last block have higher number indices (row and columns). (c) The case with the last element is shifted. (d) The case where the last two elements are shifted. (e) When we compare the submatrices which have many blocks we consider spreading of the largest sub-block, such as $m2 + m3$, first. Then, this submatrix, say $(m1; m2 + m3)$, can be connected with another submatrix, say $(m1; m2; m3)$ by considering further spreading of the second largest sub-block, such as $m3$.

holds for $n \geqslant t_1 - 1 = 0$ in the case of $|J| \in \{0,1\}$. Moreover, this matrix inequality holds for $n \geqslant t_1 - 1 = 1$ in the case of $|J| = 2$ and for $n \geqslant t_1 - 1 = 3$ in the case of $|J| = 4$. Note again that the inequality for matrices indicates all elements are non-negative.

Similarly, from the rows of $l \in \{0,1,2\}$ in Table I, we can confirm that the relation on the 3×3 submatrices,

$$\begin{pmatrix} \gamma_{n,n} & \gamma_{n,n+1} & \gamma_{n,n+2} \\ \gamma_{n+1,n} & \gamma_{n+1,n+1} & \gamma_{n+1,n+2} \\ \gamma_{n+2,n} & \gamma_{n+2,n+1} & \gamma_{n+2,n+2} \end{pmatrix} - \begin{pmatrix} \gamma_{n+1,n+1} & \gamma_{n+1,n+2} & \gamma_{n+1,n+3} \\ \gamma_{n+2,n+1} & \gamma_{n+2,n+2} & \gamma_{n+2,n+3} \\ \gamma_{n+3,n+1} & \gamma_{n+3,n+2} & \gamma_{n+3,n+3} \end{pmatrix} \geqslant 0 \quad \text{(B4)}$$

holds for $n \geqslant t_2 - 2 = 0$ in the case of $J = 0$ and for $n \geqslant t_2 - 2 = 1$ in the case of $|J| = 1$. Furthermore, the relation of Eq. (B4) holds for $n \geqslant 1$ in the case of $|J| = 2$, $n \geqslant 4 - 2 = 2$ in the case of $|J| = 3$ and $n \geqslant 7 - 2 = 5$ in the case of $|J| = 4$. In this manner, we can show that the inequality for the $k \times k$ submatrices,

$$\begin{pmatrix} \gamma_{n,n} & \cdots & \gamma_{n,n+k-1} \\ \vdots & \ddots & \vdots \\ \gamma_{n+k-1,n} & \cdots & \gamma_{n+k-1,n+k-1} \end{pmatrix} - \begin{pmatrix} \gamma_{n+1,n+1} & \cdots & \gamma_{n+1,n+k} \\ \vdots & \ddots & \vdots \\ \gamma_{n+k,n+1} & \cdots & \gamma_{n+k,n+k} \end{pmatrix} \geqslant 0 \quad \text{(B5)}$$

holds for $n \geqslant t_{l=k-1} - k + 1$.

3. Inequalities for the spreading shift

Let us consider the following inequality for the spreading shift depicted in Fig. 3(b):

$$B - B' := \begin{pmatrix} M_0 & y \\ y^t & a \end{pmatrix} - \begin{pmatrix} M_0 & y' \\ y'^t & a' \end{pmatrix} \geqslant 0, \quad \text{(B6)}$$

where M_0, a, and a' are square matrices. Suppose that the matrices in Eq. (B6) are submatrices of $A^{(J)}$ of Eq. (17) and that $J = 0$ so that properties (i) and (ii) are fulfilled. From the decreasing order on the diagonal elements and property (ii), we can show that the relation of Eq. (B6) holds when the final row and column are shifted as in Fig. 3(c) in which a and a' are diagonal elements and y and y' are single column vectors. From the decreasing order on the diagonal and first off-diagonal elements together with property (ii), we can show that the relation of Eq. (B6) holds when the final two rows and two columns are shifted as in Fig. 3(d) (here, a and a' are 2×2 matrices). Similarly, we can generate the matrix inequalities in the form of Eq. (B6) by using properties (i) and (ii) for any size of a whenever the diagonal shift ($a \to a'$) is in decreasing order.

By further spreading the last lows and columns associated with the position of the square matrix a, we can generate inequalities with more separations as in Fig. 3(e). To make the three-separation ($m1$:$m2$:$m3$), we consider the diagonal shift of the column-length $m2 + m3$ square matrix first, and then we spread the last square matrix of the column-length $m3$. We can reach any given separation by repeating these processes recursively.

From properties (i) and (ii), we can see that, for sufficiently larger n, the inequalities for the diagonal shift and spreading shift always hold. This is also the case for general $J \neq 0$ since similar properties hold with a bit of complicated conditions, such as Eq. (B3) and Table I (see the discussion in Appendix B 1). Hence, the set of submatrices we need to compare the maximum eigenvalues is a finite set of smaller-n-index submatrices that cannot be connected by the matrix inequalities obtained by these properties. On this basis, the search for the submatrices that have larger maximum eigenvalues can be carried out by a relatively small number of calculation steps. We will present a systematical procedure to identify relevant submatrices in the following.

4. Relevant set of submatrices

a. For $J = 0$ and $k \in \{1,2,3,4,5\}$

Let us suppose that $J = 0$. For $k \in \{1,2,3\}$, the matrix inequalities both in the diagonal shift and in the spreading shift of Figs. 3(a) and 3(b) hold for any $n \geqslant 0$. This leads to $\|A^{(0)}_{\{0\}}\| \geqslant \|A^{(0)}_{\{n\}}\|$ for $k = 1$, $\|A^{(0)}_{\{0,1\}}\| \geqslant \|A^{(0)}_{\{n,n'\}}\|$ for $k = 2$, and $\|A^{(0)}_{\{0,1,2\}}\| \geqslant \|A^{(0)}_{\{n,n',n''\}}\|$ for $k = 3$.

For $k = 4$, we can show the inequality for the spreading shift $\|A^{(0)}_{\{n,n+1,n+2,n+3\}}\| \geqslant \|A^{(0)}_{\{n,n+n',n+n'',n+n'''\}}\|$ by using property (ii) and the inequalities in the diagonal shift of the 2×2 and 3×3 matrices above. From the row of $l = 3$ in Table I, the inequalities for the diagonal shift are fulfilled whenever $n \geqslant t_l - l = 2$. Hence, the only submatrices that cannot be connected by the inequalities are $A^{(0)}_{\{0,1,2,3\}}$, $A^{(0)}_{\{1,2,3,4\}}$, and $A^{(0)}_{\{2,3,4,5\}}$. Therefore, the maximum in Eq. (18) is obtained by comparing the first three matrices, i.e., $\max_{n\in\{0,1,2\}} \|A^{(0)}_{\{n,n+1,n+2,n+3\}}\|$.

For $k = 5$, we can show the inequality for the spreading shift $\|A^{(0)}_{\{n,n+1,n+2,n+3,n+4\}}\| \geqslant \|A^{(0)}_{\{n,n+n',n+n'',n+n''',n+n''''\}}\|$ by using property (ii) and the results above except for the case of $n = 0$. For $n = 0$, we could not have the matrix inequality for $A^{(0)}_{\{0,1,2,3,4\}}$ and $A^{(0)}_{\{0,2,3,4,5\}}$ because the 4×4 matrix inequality cannot hold for the first two cases of the diagonal shift ($n \geqslant t_3 - 3 = 2$). From property (i) and the results of $k \leqslant 4$ above, we also have the inequality for the diagonal shift $\|A^{(0)}_{\{n,n+1,n+2,n+3,n+4\}}\| \geqslant \|A^{(0)}_{\{n+1,n+2,n+3,n+4,n+5\}}\|$ when $n \geqslant t_4 - 4 = 5$. In this case, the matrix inequality for the diagonal shift cannot hold for the first five 5×5 submatrices $\|A_{\{n,n+1,n+2,n+3,n+4\}}\|$ with $n \in \{0,1,2,3,4\}$. Therefore, the optimization can be performed by taking the largest one of $\|A_{\{0,2,3,4,5\}}\|$ and $\|A_{\{n,n+1,n+2,n+3,n+4\}}\|$ with $n \in \{0,1,2,3,4,5\}$.

b. For general J and k

For temporary simplicity, let us suppose $|J| \leqslant 4$ [it corresponds to $u^{(J)} = 0$ in Eq. (B3)]. The set of submatrices which cannot be connected by the inequalities for given k can be specified from $t_{k-1}, t_{k-2}, \ldots, t_0$ in Table I as follows: First, we generate the number of $t_{k-1} - (k-1) + 1 = t_{k-1} - k + 2$ sets of $\vec{n}$ in which the submatrix corresponding to $A_{\vec{n}}$ cannot be

connected by the inequalities with respect to the diagonal shift,

$$\begin{aligned}&\{0,1,\ldots,k-1\},\\&\{1,2,\ldots,k-1,k\},\\&\quad\vdots\\&\{t_{k-1}-k,\ldots,t_{k-1}-1\},\\&\{t_{k-1}-k+1,\ldots,t_{k-1}\}.\end{aligned}\tag{B7}$$

Second, we generate the sets by repeating the diagonal shift of the last $k-1$ elements of each set of Eq. (B7) until the last index of $\vec{n}$ fulfills $n_k > t_{k-2}$ as

$$\begin{aligned}&\{0,\underbrace{1,\ldots,k-1}_{k-1\text{ elements}}\},\{0,\underbrace{2,3,\ldots,k}_{\to\text{Shifted}}\},\{0,\underbrace{3,4,\ldots,k+1}_{\to\text{Shifted}}\},\ldots\\&\{1,\underbrace{2,\ldots,k-1,k}_{k-1\text{ elements}}\},\{1,\underbrace{3,4,\ldots,k-1,k}_{\to\text{Shifted}}\},\\&\{1,\underbrace{4,5,\ldots,k,k+1}_{\to\text{Shifted}}\},\ldots\\&\quad\vdots\\&\{t_{k-1}-k,\ldots,t_{k-1}-1\},\{t_{k-1}-k,t_{k-1}-k+2,\ldots,t_{k-1}\},\ldots\\&\{t_{k-1}-k+1,\ldots,t_{k-1}\},\{t_{k-1}-k+1,t_{k-1}-k+3,\ldots,\\&t_{k-1}+1\},\ldots\ .\end{aligned}\tag{B8}$$

Third and finally, we generate the sets by repeating the diagonal shift of the last $k-2$ elements of each set of Eq. (B8) until the last index of $\vec{n}$ fulfills $n_k > t_{k-3}$. For example, from the elements in the first line of Eq. (B8) we have

$$\begin{aligned}&\{0,1,\underbrace{2,\ldots,k-1}_{k-2\text{ elements}}\},\{0,1,\underbrace{3,4,\ldots,k}_{\to\text{Shifted}}\},\{0,1,\underbrace{4,5,\ldots,k+1}_{\to\text{Shifted}}\},\ldots\\&\{0,2,\underbrace{3,4,\ldots,k}_{k-2\text{ elements}}\},\{0,2,\underbrace{4,5,\ldots,k+1}_{\to\text{Shifted}}\},\\&\{0,2,\underbrace{5,6,\ldots,k+2}_{\to\text{Shifted}}\},\ldots\\&\{0,3,\underbrace{4,5,\ldots,k+1}_{k-2\text{ elements}}\},\{0,3,\underbrace{5,6,\cdots,k+2}_{\to\text{Shifted}}\},\ldots\\&\quad\vdots\ .\end{aligned}\tag{B9}$$

In this manner, we can obtain the total number of, at most, $\prod_{l=0}^{k-1}(t_l-l-1)$ sets of indices $\vec{n}$.

For the case of $|J| > 4$, we modify the generation process by using $u^{(J)}$ of Eq. (B3) so that the diagonal shift of the last l elements is repeated until the last index of $\vec{n}$ fulfills $n_k > \max\{t_{l-1},u^{(J)}+l-1\}$.

5. Outline for numerical calculation

Suppose that k, κ, and x are given. We first search the set of $\{A^{(J)}\}_J$ which includes $(k\times k)$-principal submatrices whose trace is greater than the conjectured maximum value $\|A^{(0)}_{\{0,1,\ldots,k-1\}}\|$. This process can be executed by only using the diagonal elements of $\{A^{(J)}\}_J$.

Next, we determine the relevant submatrices according to the process described in Appendix B 4 b for relevant J.

Lastly, the maximum eigenvalues are directly compared to determine the maximum.

[1] R. Horodecki, P. Horodecki, M. Horodecki, and K. Horodecki, Quantum entanglement, Rev. Mod. Phys. **81**, 865 (2009).

[2] J.-W. Pan, Z.-B. Chen, C.-Y. Lu, H. Weinfurter, A. Zeilinger, and M. Żukowski, Multiphoton entanglement and interferometry, Rev. Mod. Phys. **84**, 777 (2012).

[3] B. M. Terhal and P. Horodecki, Schmidt number for density matrices, Phys. Rev. A **61**, 040301 (2000).

[4] S. Huang, Schmidt number for quantum operations, Phys. Rev. A **73**, 052318 (2006).

[5] D. Chruściński and A. Kossakowski, On partially entanglement breaking channels, Open Syst. Information Dyn. **13**, 17 (2006).

[6] R. Namiki, Composability of partial-entanglement-breaking channels via entanglement-assisted local operations and classical communication, Phys. Rev. A **88**, 064301 (2013).

[7] M. Horodecki, P. W. Shor, and M. B. Ruskai, Entanglement Breaking Channels, Rev. Math. Phys. **15**, 629 (2003).

[8] A. S. Holevo, Entanglement-breaking channels in infinite dimensions, Probl. Inf. Transm. **44**, 171 (2008).

[9] R. Namiki and Y. Tokunaga, Schmidt-number benchmark for genuine quantum memories and gates, Phys. Rev. A **85**, 010305(R) (2012).

[10] A. Sanpera, D. Bruß, and M. Lewenstein, Schmidt-number witnesses and bound entanglement, Phys. Rev. A **63**, 050301 (2001).

[11] Y. Tokunaga, T. Yamamoto, M. Koashi, and N. Imoto, Fidelity estimation and entanglement verification for experimentally produced four-qubit cluster states, Phys. Rev. A **74**, 020301(R) (2006).

[12] Y. Tokunaga, S. Kuwashiro, T. Yamamoto, M. Koashi, and N. Imoto, Generation of High-Fidelity Four-Photon Cluster State and Quantum-Domain Demonstration of One-Way Quantum Computing, Phys. Rev. Lett. **100**, 210501 (2008).

[13] R. Inoue, T. Yonehara, Y. Miyamoto, M. Koashi, and M. Kozuma, Measuring Qutrit-Qutrit Entanglement of Orbital Angular Momentum States of an Atomic Ensemble and a Photon, Phys. Rev. Lett. **103**, 110503 (2009).

[14] C.-M. Li, K. Chen, A. Reingruber, Y.-N. Chen, and J.-W. Pan, Verifying Genuine High-Order Entanglement, Phys. Rev. Lett. **105**, 210504 (2010).

[15] J. Sperling and W. Vogel, Determination of the schmidt number, Phys. Rev. A **83**, 042315 (2011).

[16] R. Namiki and Y. Tokunaga, Discrete Fourier-Based Correlations for Entanglement Detection, Phys. Rev. Lett. **108**, 230503 (2012).

[17] F. Shahandeh, J. Sperling, and W. Vogel, Operational Gaussian Schmidt-number witnesses, Phys. Rev. A **88**, 062323 (2013).

[18] A. J. Gutiérrez-Esparza, W. M. Pimenta, B. Marques, A. A. Matoso, J. Sperling, W. Vogel, and S. Pádua, Detection of nonlocal superpositions, Phys. Rev. A **90**, 032328 (2014).
[19] S. L. Braunstein and P. van Loock, Quantum information with continuous variables, Rev. Mod. Phys. **77**, 513 (2005).
[20] K. Hammerer, A. S. Sørensen, and E. S. Polzik, Quantum interface between light and atomic ensembles, Rev. Mod. Phys. **82**, 1041 (2010).
[21] C. Weedbrook, S. Pirandola, R. García-Patrón, N. J. Cerf, T. C. Ralph, J. H. Shapiro, and S. Lloyd, Gaussian quantum information, Rev. Mod. Phys. **84**, 621 (2012).
[22] A. Furusawa, J. L. Sørensen, S. L. Braunstein, C. A. Fuchs, H. J. Kimble, and E. S. Polzik, Unconditional quantum teleportation, Science **282**, 706 (1998).
[23] B. Julsgaard, J. Sherson, J. I. Cirac, J Fiurasek, and E. S. Polzik, Experimental demonstration of quantum memory for light, Nature (London) **432**, 482 (2004).
[24] M. Lobino, C. Kupchak, E. Figueroa, and A. I. Lvovsky, Memory for Light as a Quantum Process, Phys. Rev. Lett. **102**, 203601 (2009).
[25] S. L. Braunstein, C. A. Fuchs, and H. J. Kimble, Criteria for continuous-variable quantum teleportation, J. Mod. Opt. **47**, 267 (2000).
[26] K. Hammerer, M. M. Wolf, E. S. Polzik, and J. I. Cirac, Quantum Benchmark for Storage and Transmission of Coherent States, Phys. Rev. Lett. **94**, 150503 (2005).
[27] R. Namiki, M. Koashi, and N. Imoto, Fidelity Criterion for Quantum-Domain Transmission and Storage of Coherent States Beyond the Unit-Gain Constraint, Phys. Rev. Lett. **101**, 100502 (2008).
[28] T. Takano, M. Fuyama, R. Namiki, and Y. Takahashi, Continuous-variable quantum swapping gate between light and atoms, Phys. Rev. A **78**, 010307(R) (2008).
[29] R. Namiki, Fundamental quantum limits on phase-insensitive linear amplification and phase conjugation in a practical framework, Phys. Rev. A **83**, 040302(R) (2011).
[30] G. Chiribella and J. Xie, Optimal Design and Quantum Benchmarks for Coherent State Amplifiers, Phys. Rev. Lett. **110**, 213602 (2013).
[31] R. Namiki, Simple proof of the quantum benchmark fidelity for continuous-variable quantum devices, Phys. Rev. A **83**, 042323 (2011).
[32] Y. Yang, G. Chiribella, and G. Adesso, Certifying quantumness: Benchmarks for the optimal processing of generalized coherent and squeezed states, Phys. Rev. A **90**, 042319 (2014).
[33] R. Namiki, Converting separable conditions to entanglement breaking conditions, arXiv:1503.07109.
[34] C. A. Fuchs and M. Sasaki, Squeezing quantum information through a classical channel: measuring the quantumness of a set of quantum states, Quantum Inf. Comput. **3**, 377 (2003).
[35] R. Namiki, Verification of the quantum-domain process using two nonorthogonal states, Phys. Rev. A **78**, 032333 (2008).
[36] H. Häseler, T. Moroder, and N. Lütkenhaus, Testing quantum devices: Practical entanglement verification in bipartite optical systems, Phys. Rev. A **77**, 032303 (2008).
[37] H. Häseler and N. Lütkenhaus, Probing the quantumness of channels with mixed states, Phys. Rev. A **80**, 042304 (2009).
[38] M. Owari, M. B. Plenio, E. S. Polzik, A. Serafini, and M. M. Wolf, Squeezing the limit: quantum benchmarks for the teleportation and storage of squeezed states, New J. Phys. **10**, 113014 (2008).
[39] R. Namiki and K. Azuma, Quantum Benchmark via an Uncertainty Product of Canonical Variables, Phys. Rev. Lett. **114**, 140503 (2015).
[40] R. Namiki, Amplification uncertainty relation for probabilistic amplifiers, Phys. Rev. A **92**, 032326 (2015).
[41] N. Killoran and N. Lütkenhaus, Strong quantitative benchmarking of quantum optical devices, Phys. Rev. A **83**, 052320 (2011).
[42] N. Killoran, M. Hosseini, B. C. Buchler, P. K. Lam, and N. Lütkenhaus, Quantum benchmarking with realistic states of light, Phys. Rev. A **86**, 022331 (2012).
[43] I. Khan, C. Wittmann, N. Jain, N. Killoran, N. Lütkenhaus, C. Marquardt, and G. Leuchs, Optimal working points for continuous-variable quantum channels, Phys. Rev. A **88**, 010302 (2013).
[44] M. E. Shirokov, Schmidt number and partially entanglement-breaking channels in infinite-dimensional quantum systems, Mathematical Notes **93**, 766 (2013).
[45] M. Yukawa, H. Benichi, and A. Furusawa, High-fidelity continuous-variable quantum teleportation toward multistep quantum operations, Phys. Rev. A **77**, 022314 (2008).
[46] S. Pirandola, J. Eisert, C. Weedbrook, A. Furusawa, and S. L. Braunstein, Advances in quantum teleportation, Nat. Photonics **9**, 641 (2015).
[47] T. Ralph and A. Lund, in *Quantum Communication Measurement and Computing: Ninth International Conference on QCMC*, edited by A. Lvovsky, AIP Conf. Proc. No. 1110 (AIP, New York, 2009), p. 155.
[48] H. M. Chrzanowski, N. Walk, S. M. Assad, J. Janousek, S. Hosseini, T. C. Ralph, T. Symul, and P. K. Lam, Measurement-based noiseless linear amplification for quantum communication, Nat. Photonics **8**, 333 (2014).
[49] G. Y. Xiang, T. C. Ralph, A. P. Lund, N. Walk, and G. J. Pryde, Heralded noiseless linear amplification and distillation of entanglement, Nat. Photonics **4**, 316 (2010).
[50] J. S. Neergaard-Nielsen, Y. Eto, C. W. Lee, H. Jeong, and M. Sasaki, Quantum tele-amplification with a continuous-variable superposition state, Nat. Photonics **7**, 439 (2013).
[51] R. A. Horn and C. R. Johnson, *Matrix Analysis* (Cambridge University Press, New York, 2007).